Journal of Inorganic Biochemistry 141 (2014) 28–35

Contents lists available at ScienceDirect

Journal of Inorganic Biochemistry

journal homepage: www.elsevier.com/locate/jinorgbio

Decomposition of amino diazeniumdiolates (NONOates): Molecular mechanisms

Nizamuddin Shaikh [a], Marat Valiev [b], Sergei V. Lymar [a,*]

[a] Chemistry Department, Brookhaven National Laboratory, Upton, NY 11973, United States
[b] William R. Wiley Environmental Molecular Sciences Laboratory, Pacific Northwest National Laboratory, P.O. Box 999, Richland, WA 99352, United States

ARTICLE INFO

Article history:
Received 9 February 2014
Received in revised form 12 August 2014
Accepted 13 August 2014
Available online 23 August 2014

Keywords:
Diazeniumdiolates
NONOates
NO donor
Mechanism
Tautomerization
Ab initio calculations

ABSTRACT

Although diazeniumdiolates ($X[N(O)NO]^-$) are extensively used in biochemical, physiological, and pharmacological studies due to their ability to release NO and/or its congeneric nitroxyl, the mechanisms of these processes remain obscure. In this work, we used a combination of spectroscopic, kinetic, and computational techniques to arrive at a quantitatively consistent molecular mechanism for decomposition of amino diazeniumdiolates (amino NONOates: $R_2N[N(O)NO]^-$, where R = $-N(C_2H_5)_2$ (**1**), $-N(C_3H_4NH_2)_2$ (**2**), or $-N(C_2H_4NH_2)_2$ (**3**)). Decomposition of these NONOates is triggered by protonation of their $[NN(O)NO]^-$ group with the apparent pK_a and decomposition rate constants of 4.6 and 1 s^{-1} for **1**; 3.5 and 0.083 s^{-1} for **2**; and 3.8 and 0.0033 s^{-1} for **3**. Although protonation occurs mainly on the O atoms of the functional group, only the minor $R_2N(H)N(O)NO$ tautomer (population ~10^{-7}, for **1**) undergoes the N–N heterolytic bond cleavage (k_d ~ 10^7 s^{-1} for **1**) leading to amine and NO. Decompositions of protonated amino NONOates are strongly temperature-dependent; activation enthalpies are 20.4 and 19.4 kcal/mol for **1** and **2**, respectively, which includes contributions from both the tautomerization and bond cleavage. The bond cleavage rates exhibit exceptional sensitivity to the nature of R substituents which strongly modulate activation entropy. At pH < 2, decompositions of all three NONOates that have been investigated are subject to additional acid catalysis that occurs through di-protonation of the $[NN(O)NO]^-$ group.

1. Introduction

A growing appreciation of the biological and pharmacological roles of nitric oxide (NO) and nitroxyl (HNO/NO^-) has naturally rekindled interest in diazeniumdiolates, the compounds of the general structure $X\text{-}[N(O)NO]^-$ shown in Scheme 1 [1–6]. Based on their known decomposition pathways, these compounds can be viewed either as adducts of X-NO with NO^- or as complexes of Lewis bases X^- with a Lewis acid N_2O_2, an N–N dimer of NO. The latter view is somewhat more instructive because it captures the origin of the N_2O_2 stabilization in diazeniumdiolates.

An N–N bond in ONNO is extremely weak, but the addition of an electron dramatically stabilizes the resulting hyponitrite radical ($ONNO^-$); effectively, the extra electron "glues" together the two NO fragments [7–10]. Addition of another electron yields an even more stable hyponitrite di-anion ($ONNO^{2-}$) [11]. The ONNO stabilization in all other diazeniumdiolates is achieved in the same manner by adding an electron pair donor X^-. As has been extensively reviewed [2], most frequently X^- is a carbanion or amide anion but diazeniumdiolates with $X^- = O^{2-}$ (as in Angeli's salt) or SO_3^{2-} (as in Pelouze's salt) are also long-known. From this perspective, both $ONNO^-$ and $ONNO^{2-}$ should be accepted as diazeniumdiolates with X^- being an electron and electron pair, respectively, and the ON-$[N(O)NO]^-$ anion [8,10,12] should be recognized as a *bona fide* nitroxy diazeniumdiolate with $X^- = NO^-$.

Decomposition of diazeniumdiolates can be triggered either by photoexcitation [13,14] or by the addition of an electron pair acceptor that counters the stabilization exerted by X^-; commonly, a proton can play this role. Depending on the nature of X^-, this destabilization by H^+ can result in decomposition to various products as shown in Scheme 1. However, the molecular mechanisms of these reactions remain obscure; in most cases a rate determining step has not been unambiguously established and quantitatively characterized. This lack of mechanistic understanding hampers our ability to manipulate diazeniumdiolates toward the desired properties.

Of all diazeniumdiolates, the amino variety with $X^- = R_1R_2N^-$ is the most extensively used in biochemical, physiological, and pharmacological studies due to their ability to release NO in neutral media

$$R_2NN(O)NO^- + H^+ \rightarrow R_2NH + 2NO. \quad (1)$$

These compounds are often called amino NONOates, and we will use this notation throughout this paper. Despite a wealth of phenomenology consisting primarily of the decomposition rates and NO yields under the physiological medium conditions and of comparative studies for a

* Corresponding author. Tel.: +1 631 344 4333; fax: +1 631 344 5815.
E-mail address: Lymar@bnl.gov (S.V. Lymar).

http://dx.doi.org/10.1016/j.jinorgbio.2014.08.008
0162-0134/

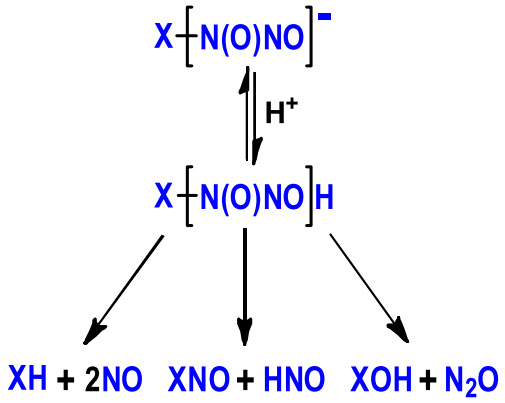

Scheme 1. General structure and known decomposition pathways of NONOates.

large number of amino NONOates [1,2,15–20], we are aware of only a few credible attempts at understanding the underlying molecular mechanisms [21–26]. Unfortunately, these attempts generally suffer from the lack of complete pH dependencies for rates and from the data interpretation inconsistencies that we will briefly address in the Discussion section. In this work, we present a mechanistic investigation of the amino NONOates shown in Scheme 2. Through a combination of spectroscopic, kinetic, and computational techniques, we arrive at a quantitatively consistent molecular mechanism for reaction 1 and discuss the main factors determining its rate.

2. Materials and methods

2.1. Materials

Analytical grade chemicals and Milli-Q purified (ASTM type I) water were used throughout. D_2O (99.8%) was obtained from ICN Biomedicals. Anionic diethylamine NONOate (**1**, diethylammonium salt) and zwitterionic dipropylenetriamine NONOate (**2**) and diethylenetriamine NONOate (**3**) from Cayman Chemical were used as received. Their stock solutions were prepared in 1–10 mM NaOH and stored on ice. Concentrations of these solutions were determined spectrophotometrically using molecular absorptivities $\varepsilon_{248} = 8.89 \times 10^3$ for **1** [20], $\varepsilon_{252} = 7.86 \times 10^3$ for **2**, and $\varepsilon_{252} = 7.64 \times 10^3\ M^{-1}\ cm^{-1}$ for **3** [16].

2.2. Experimental procedures

Spectrophotometric pH titrations were carried out using a Cary 500 spectrophotometer (Varian). To avoid concentration changes due to the NONOate decompositions during spectral scans that become significant at low pH, a syringe-driven mixing system was employed in which an alkaline NONOate solution was mixed with a desired buffer and the spectra were recorded under continuous flow conditions. The buffer used were: 0.01 M borate for pH 10–8, 0.1 M phosphate for pH 8–6, 0.01 M acetate for pH 5–3.7, 0.1 M phosphate for pH 3.5–2.6, and $HClO_4$ for pH 2–0.

The NONOate decomposition kinetics were measured under thermal stabilization at 25 °C (except for the activation measurements) and strictly anaerobic conditions in a head-space-free flow optical cell. For the sufficiently slow reactions the above-described flow system and Cary 500 were adequate, but the faster reactions were measured using SX20 stopped flow spectrometer (Applied Photophysics).

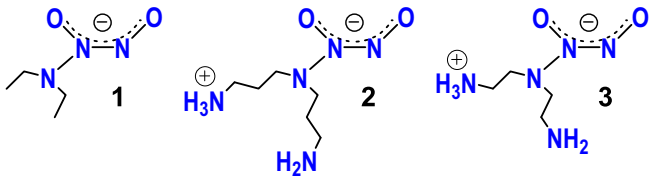

Scheme 2. Amino NONOates investigated in this work.

2.3. Computational techniques

Calculations were performed with the NWChem computational chemistry package [27] and consisted of two stages. In the first stage, quantum mechanical/molecular mechanics (QM/MM) approach was used for structural characterization of the NONOate species in aqueous environment. The QM/MM approach implemented in NWChem follows standard electrostatic embedding scheme with no modifications of the classical force parameters, and its performance has been validated for various aqueous systems [28–32]. In the second stage, hydration free energies for the configurations obtained in the first stage were evaluated with the self-consistent reaction field theory of Klamt and Schüürmann (COSMO) [33].

The system for QM/MM calculations consisted of a NONOate molecule placed in 30 Å cubic box of classical water molecules. The QM region containing only NONOate was treated at the density functional level of theory (DFT/B3LYP [34]) with 6-31+G* basis set [35]. The rest of the system (in this case, all the water molecules) was treated classically using SPC/E [36] water model and the periodic boundary conditions based on the cutoff radius of 10 Å. Within this general scheme, the following procedure for structural QM/MM calculations was employed. First, an initial guess was generated either by hydrating a gas-phase solute structure using NWChem prepare module or by modifications of previously optimized aqueous structure; e.g., the initial guess for decomposition products was obtained by stretching the corresponding N – N bond in the optimized aqueous reactant. With the initial structure constructed, the QM/MM optimization of the entire system was performed [31]. Then, with the NONOate structure fixed, the surrounding solvent was equilibrated for 100 ps at 25 °C using classical molecular dynamics calculations. This step was followed by another round of QM/MM optimization of the entire system.

To determine the NONOate decomposition pathway, we used the optimized structures of both hydrated reactant and product in conjunction with the previously developed QM/MM implementation [31] of the nudged elastic band (NEB) method [37]. The transition state was obtained as the highest energy structure on the 10-bead NEB path, and the QM/MM calculations were performed to verify the presence of the single imaginary vibrational mode in this structure, which is a transition state indicator.

The solute aqueous free energy was obtained as $G = E + H_c - TS + \Delta G_h + 1.84$ kcal/mol, where E is the electronic contribution to internal energy computed in the gas phase at CCSD(T) level of theory [38] and maug-cc-pVTZ basis set [39], H_c is the usual thermal enthalpy correction, TS accounts for the solute entropy contribution, ΔG_h contains the free energy of hydration from COSMO calculations, and the last term accounts for the standard state change from 1 bar pressure to 1 M concentration. Notably, both H_c and S were computed for the solute structure and vibrational frequencies produced by the QM/MM model. For the COSMO calculations of ΔG_h, we used 78.0 for water dielectric constant and solvation cavity defined by a set of intersecting atomic spheres with radii suggested by Stefanovich and Truong (N 2.126, H 1.172, O 1.576, and C 1.635 Å) [40]. The QM theory in COSMO calculations was identical to that used for QM/MM calculations, namely DFT/B3LYP with 6-31+G* basis set.

As a test of this method for the free energy computations, we performed a tautomer analysis for nitramide that resembles NONOates in terms of its structure and chemical composition, and for which the free energy gap of 8.2 kcal/mol between its major *nitro*-tautomer (H_2N-NO_2) and the higher energy *aci*-tautomer (HN═N(O)OH) had been reliably estimated from experiment [41]. Our computations gave 8.3 kcal/mol (Table S1 and Fig. S3), which is nearly exact match with the experimental value. Even if somewhat serendipitous, this match

does give us a measure of confidence in the employed computational technique.

3. Results

3.1. Acid–base equilibria

Complete and accurate quantitative description of protonation states is essential for understanding the pH-dependent decomposition of NONOates. Chemical intuition suggests that the terminal amines in **2** and **3** are the most basic sites in these NONOates. Because the two amino groups are well-separated, we should expect that each amine is protonated independently, and, for statistical reasons, the first apparent pK_{a1} should be 0.3 units lower than the second pK_{a2}. These expectations are wholly confirmed by the titration data in Fig. 1. Upon dissolution of solid **2** and **3** that are zwitterions with half-protonated terminal amines, a buffered solution is obtained with pH = pK_{a2} = 9.2, which consumes one acid equivalent on titration to pH 7 with the mid-point at pH = pK_{a1} = 8.9. Thus at pH 7, **2** and **3** each carry a unit positive charge, whereas **1** carries a unit negative charge.

In addition to charging, protonation of terminal amines slightly perturbs the $[N(O)NO]^-$ chromophoric group as evidenced by a ~2 nm red shift in the spectrum of **3** on lowering pH from 12 to 7 (Fig. 1, inset). A very similar spectral change was observed for **2** but not for **1** that lacks terminal amines. However, apart from this indirect influence, protonation of terminal amines is not involved in the decomposition of **2** and **3**, as discussed below.

Much larger spectral changes are observed for all three NONOates at pH < 7. These pH-dependent changes exhibit all the hallmarks of protonation of the chromophoric $[N(O)NO]^-$ group; that is, a significant blue shift with decrease of absorption maximum upon protonation and the isosbestic point as shown for **1** in Fig. 2A. The fits of the theoretical titration equation

$$\varepsilon_{app} = \frac{\varepsilon_a K_{mp} + \varepsilon_{mp}[H^+]}{K_{mp} + [H^+]} \quad (2)$$

to the titration curves yielded $pK_{mp} = 4.6 \pm 0.1$ (Fig. 2B). Here, ε_a and ε_{mp} are the molar absorptivities of the anion and the conjugate mono-protonated species and K_{mp} is the attendant acid dissociation constant. Similar spectral and titration curves were observed for **2** and **3** (Figs. S1 and S2), and their corresponding pK_a were determined as 3.8 ± 0.1 and 3.5 ± 0.1.

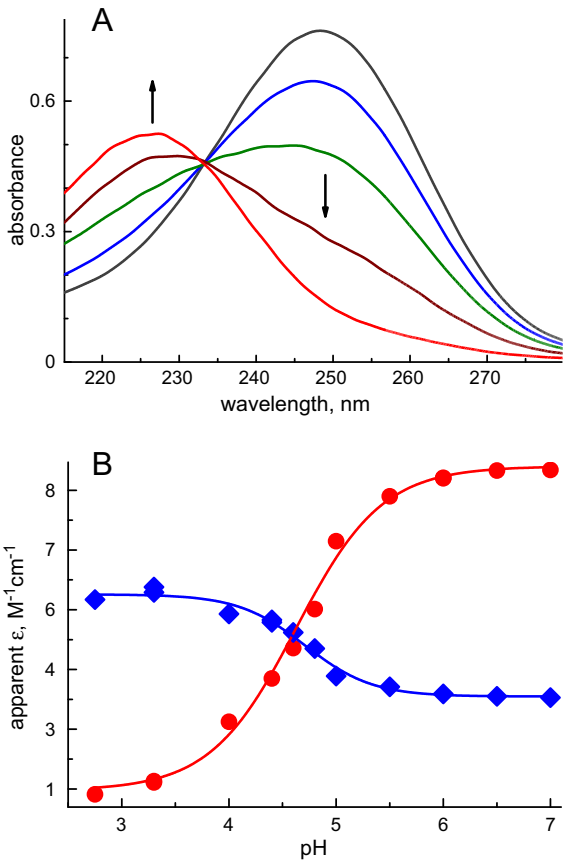

Fig. 2. Panel A: changes of **1** absorption spectra upon lowering pH from 7.0 to 5.0, 4.8, 4.0, 3.3. Isosbestic point is observed at 233 nm. Panel B: pH dependencies of the apparent molar absorptivities at 248 nm (red circles) and 226 nm (blue diamonds); the lines show fits to Eq. (2) with pK_{mp} = 4.6 (red) and 4.7 (blue). (For interpretation of the references to color in this figure legend, the reader is referred to the web version of this article.).

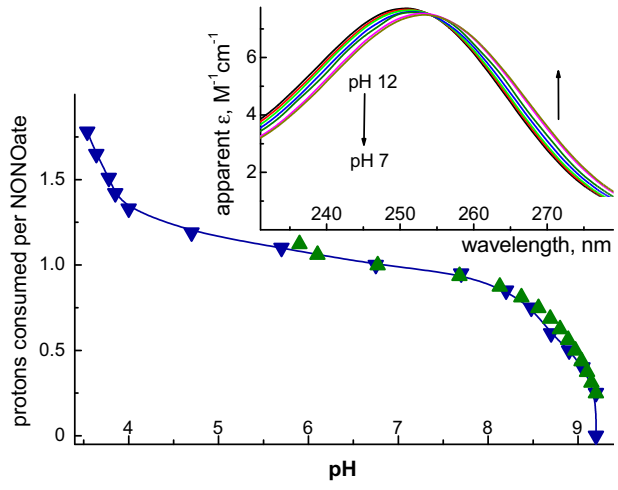

Fig. 1. pH-metric titrations of **2** (green up triangles) and **3** (blue down triangles). Solid NONOates were dissolved in 5 mL of pure water to give 5 mM solutions of pH 9.2 that were titrated with 25 mM HCl. On the acidic side, these measurements were limited by the rates of NONOate decompositions. Inset: spectral shift for **3** upon changing pH from 12 to 7. (For interpretation of the references to color in this figure legend, the reader is referred to the web version of this article.).

Because the spectrophotometric titration gives no information about the protonation site, we have resorted to computational methods for ranking the five possible tautomers of protonated **1** in terms of their relative energies in aqueous environment. Fig. 3 shows the computed optimized structures for **1** and the tautomers of **1**-H, and Table 1 summarizes their geometry and energetics. (See, Table S1 for the more details.) Recalling that the nominal bond lengths for N–N, N=N, N–O, and N=O are 1.45, 1.25, 1.40, and 1.21 Å, respectively [43] we observe that the O1–N2, N2–N3, and N3–O4 bonds in the anion can all be best characterized as partially double, which corresponds to the Lewis structures that we use in Scheme 2 and in Fig. 3. Notably, the N2–N3 double bond character gives rise to the E and Z isomers, and the calculations reveal that the lowest energy structures are all Z isomers. However for the **1**-H(5) species, we have found that the E isomer is only slightly (0.7 kcal/mol) above the corresponding Z isomer (Fig. S4), and this energy difference is likely to be within the computational uncertainty. The most consequential structural features of the mono-protonated species in Table 1 are that their N3–N5 bond is essentially single for all tautomers and, with the exception of very high energy **1**-H(3), the N2–N3 bond remains partially double. Lewis structures that best correspond to the computed ones are included in Fig. 3. As can be seen from the bottom lines in Table 1, comparison between our computed structure and the crystallographic data is very favorable, which serves to validate our structural computations.

As expected and in agreement with previous computations [21,23], protonation at oxygen atoms is preferential with the terminal O1

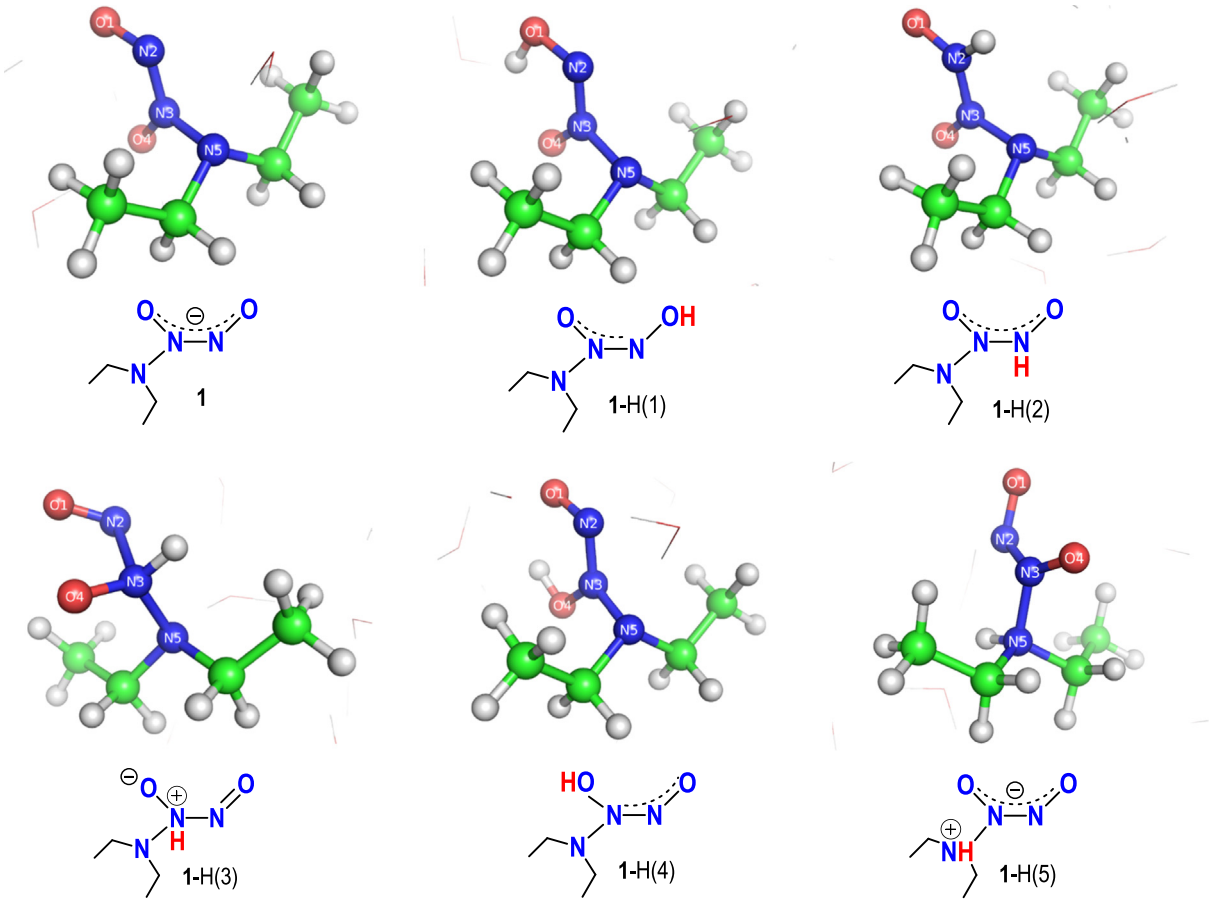

Fig. 3. Optimized structures of the hydrated **1** anion and its mono-protonated tautomers showing surrounding water molecules. Also shown are the corresponding Lewis structures based on bond lengths in Table 1. Top to bottom and left to right: **1**, **1**-H(1), **1**-H(2), **1**-H(3), **1**-H(4), and **1**-H(5).

being the most basic site followed by the O4 site. Among the nitrogen sites, protonation of N5 is most advantageous leading to overall third lowest energy tautomer **1**-H(5). The apparent K_{mp} derived from the data in Fig. 2 relates to the K_a values of individual tautomers through

$$\frac{1}{K_{mp}} = \sum_{i=1}^{i=5} \frac{1}{K_a(\mathbf{1}\text{-H}(i))} = \frac{1}{K_a(\mathbf{1}\text{-H}(1))} \sum_{i=1}^{i=5} F_i \qquad (3)$$

where $F_i = K_a(\mathbf{1}\text{-H}(1)) / K_a(\mathbf{1}\text{-H}(i)) = \exp(-\Delta G_i/RT)$ are the fractions of individual tautomers. From this equation and ΔG_i in Table 1, we estimate: $pK_a(\mathbf{1}\text{-H}(2)) \approx -5.9$, $F_2 \approx 3 \times 10^{-11}$; $pK_a(\mathbf{1}\text{-H}(3)) \approx -15$, $F_3 \approx 6 \times 10^{-20}$; $pK_a(\mathbf{1}\text{-H}(4)) \approx 1.7$, $F_4 \approx 10^{-3}$; and $pK_a(\mathbf{1}\text{-H}(5)) \approx -2.8$, $F_5 \approx 6 \times 10^{-8}$. A comparison of $pK_a \approx -2.8$ for the **1**-H(5) tautomer with $pK_a = -2.0$ for N-cyanodiethylammonium [44] suggests that, despite its overall negative charge, the $-[N(O)NO]^-$ group is as strongly electron-withdrawing as the –CN group; the substitution of diethylammonium ($pK_a = 10.8$ [45]) with either of these groups increases its acidity by ~13 units. The $-[N(O)NO]^-$ group is, in fact, the hyponitrite radical [7,9], and its considerable electron-withdrawing strength is consistent with the high reduction potential $E^0 = 0.96$ V vs. NHE of this radical [7], which exerts large polarization (inductive effect) on the N3–N5 σ-bond in **1**-H(5).

3.2. Decomposition kinetics

These are conveniently observed through the decay of the strong UV absorption bands of the NONOates. In qualitative agreement with the

Table 1
Computed properties of the lowest energy structures for hydrated **1** and tautomers of **1**-H shown in Fig. 3.

Species	Relative ΔG_i, kcal/mol	Bond length, Å				Bond angles, degrees		
		O1–N2	N2–N3	N3–O4	N3–N5	O1–N2–N3	N2–N3–O4	N5–N3–O4
1-H(1)	0.00	1.36	1.28	1.27	1.43	111	125	121
1-H(2)	14.3	1.26	1.30	1.25	1.44	124	123	123
1-H(3)	26.3	1.15	1.85	1.28	1.47	105	111	119
1-H(4)	4.0	1.24	1.31	1.40	1.38	114	121	118
1-H(5)	10.0	1.28	1.30	1.28	1.51	115	133	116
1		1.28	1.30	1.30	1.44	115	128	119
1, Na^+		1.29	1.29	1.31	1.42	113	126	121
1, $Et_2NH_2^+$		1.32	1.28	1.28	1.43	112	126	120

The bottom two lines show crystallographic data for the salts of **1** [42].

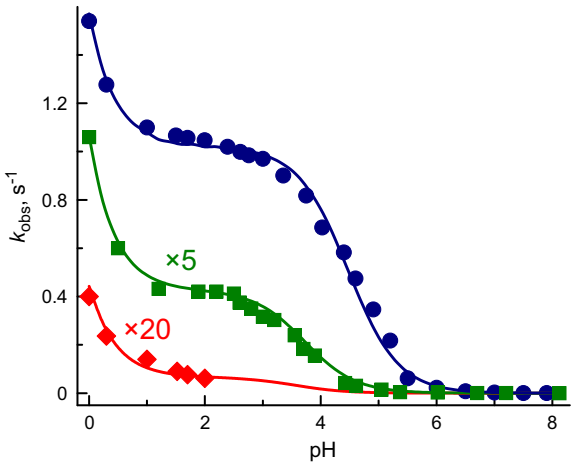

Fig. 4. pH dependencies of the observed rate constants for **1** (blue circles), **2** (green squares) and **3** (red diamonds). For **2** and **3** the k_{obs} data are multiplied by 5 and 20, respectively. The curves show fits to Eq. (4) with the parameters from Table 2. (For interpretation of the references to color in this figure legend, the reader is referred to the web version of this article.).

previous reports [17,22], the decays show a very good exponential behavior, and a sharp increase in the decay rate as the N(O)NO$^-$ groups of the NONOates becomes protonated (Fig. 4). However, the rate constants do not completely level off, and we observe a previously unreported further steep increase in rates at lower pH. A control experiment has shown that the rate enhancement in the high acid concentration region (0.001–1 M HClO4) is not due to the ionic strength effect. The addition of 1 M $NaClO_4$ at pH 1.0 (0.1 M $HClO_4$) resulted only in a 6% rate increase for **1**; thus, high medium acidity opens an additional decay pathway. This feature is consistent with the onset of the second protonation that further decreases the NONOate stability.

The most generic mechanism describing this behavior is shown in Scheme 3 which corresponds to the following expression for the observed rate constant

$$k_{obs} = \frac{k_{mp}[H^+] + \frac{k_{dp}}{K_{dp}}[H^+]^2}{K_{mp} + [H^+] + \frac{1}{K_{dp}}[H^+]^2} \quad (4)$$

where K_{dp} and K_{mp} are the acid dissociation constants and k_{dp} and k_{mp} are the rate constants for decomposition of a NONOate with diprotonated and mono-protonated functional groups, respectively. This

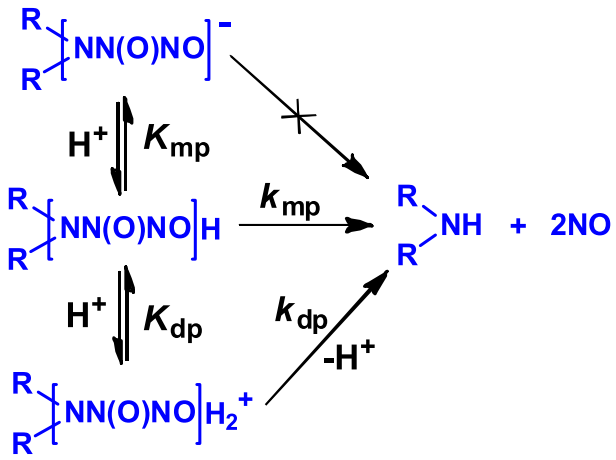

Scheme 3. Proton-assisted decomposition of amino NONOates.

equation faithfully describes the entire pH dependencies in Fig. 4 for both **1** and **2** and the low pH rate increase for **3** (the higher pH kinetics for **3** were deemed rather uninformative and not studied for this very stable NONOate). It is clear from the data that in all cases $k_{dp} \gg k_{mp}$ and that pK_{dp} is negative making the last denominator term in Eq. (4) small even at pH ~0. Therefore, only the k_{dp}/K_{dp} ratios, k_{mp}, and pK_m could be determined from the data, and these are shown in Table 2.

Temperature dependencies of the decay rates were investigated for **1** and **2** at pH 2; that is, when the functional groups of these NONOates are completely mono-protonated and yet the contribution to rate from the k_{dp} pathway is still negligible as it is obvious in Fig. 4. Under these conditions, k_{obs} is essentially identical with k_{mp} (Eq. (4)). As can be seen from Fig. 5 and Table 2, the decomposition of mono-protonated species occurs with very significant activation energy that is practically identical for **1** and **2** and the lower rate for **2** is entirely due to the much lower pre-exponential factor. Our E_a value for **1** is in general agreement with a crude estimate of 24 kcal/mol obtained by Ramamurthi and Lewis [17].

The hydrogen kinetic isotope effect (*KIE*) was measured for **2** by running its decomposition in acidic H_2O and D_2O under the otherwise identical conditions. The values for $KIE = k_{mp}(H_2O) / k_{mp}(D_2O) = 0.82$ and 0.85 were found in 10 and 20 mM $HClO_4$, respectively. These numbers indicate that the isotope effect is secondary [46] and inverse ($KIE < 1$); that is, a hydrogen ion is not directly involved in the decomposition of mono-protonated species and the measured reaction is likely to be not elementary.

4. Discussion

Apart from the pH region above 6 where the amino end-groups of **2** and **3** undergo the acid–base equilibration (Fig. 1), the protonation and attendant decomposition patterns for all three NONOates are similar (Scheme 3). It is clear from Table 2 that summarizes our kinetic data that there is a good correspondence between spectrally and kinetically determined pK_{mp} values, as it should be if Scheme 3 is valid. This is in variance with the previous report by Davies and co-workers who, as shown in Table 2, found spectrally determined pK_a values consistently much lower than pK_a obtained from kinetics. To explain this observation, they suggested two protonation steps at the [NN(O)NO]$^-$ group between pH 8 and 2, both leading to rate increases but only that occurring at lower pH reflected in the UV spectrum. Our data in Figs. 1, 2, and 4 clearly show that this is not the case: in this pH range, there is only one protonation step affecting both kinetics and spectrum.

We will now consider the molecular mechanism of decomposition of amino NONOates, focusing primarily on the mono-protonated species and compound **1** as a prototypical case. First, we note that the plateaus for k_{obs} around pH 2 in Fig. 4 and the very small inverse hydrogen kinetic isotope effect that we have observed exclude from consideration any mechanism with proton participation in the rate-determining step including the tautomerization reaction and the mechanism proposed in the theoretical work by Hall and co-workers [21]. Thus, the rate-determining step must be the monomolecular decomposition of one (or, less likely, more than one) of the **1**-H tautomers shown in Fig. 3. As for the equilibration between tautomers, its mechanism undoubtedly involves deprotonation–protonation with intermediacy of the **1** anion (see Scheme S1). Because the distribution of tautomer populations at equilibrium is pH-independent, the experimentally observable values k_{mp} and K_{mp} (defined by Eqs. (3) and 4) are related to the monomolecular decomposition rate constants, $k_d(i)$, of tautomers and their acidities, $K_a(i)$, as

$$k_{mp} = \sum_{i=1}^{i=5} \frac{K_{mp}}{K_a(i)} k_d(i). \quad (5)$$

Recalling that $k_{mp} = 1\ s^{-1}$ and $pK_{mp} = 4.6$, we estimate that tautomers with pK_a more negative than −4.5 cannot appreciably contribute

Table 2
Kinetic parameters for decompositions of amino NONOates.[a]

Species	pK_{mp}[b]	k_{mp},[b] s^{-1}	$t_{½}$,[c] min at pH 7	k_{dp}/K_{dp},[b] M^{-1} s^{-1}	A, 10^{13} s^{-1}	$\Delta S^{\#}$, cal/(mol K)	E_a ($\Delta H^{\#}$), kcal/mol	pK_a from ref. [22]
1	4.5 (4.6[d])	1.0	3.7	0.57	330	14.5	21 (20.4)	5.0 (4.5[d])
2	3.6 (3.5[d])	0.083	350	0.13	4.0	5.7	20 (19.4)	nd
3	3.7 (3.8[d])	0.0033	7000	0.019	nd	nd	nd	5.9 (3.1[d])

[a] Parameters are defined in Eq. (4).
[b] At 25 °C.
[c] Half-life estimated using Eq. (4) and parameters in the table.
[d] Spectroscopically determined pK_a.

to the decomposition with the observed rate (see Scheme S1 and its discussion), and we can safely exclude decomposition pathways through the highest energy **1**-H(2) and **1**-H(3) tautomers.

From the bond lengths in Table 1 and the related discussion of their structural implications we believe that the lowest energy pathways to the amine and NO final products are through the rate determining step that involves heterolytic scission of the N3–N5 single bond in one of the three remaining tautomers as shown in Scheme 4. While for **1**-H(5) such a pathway gives relatively low-energy Et_2NH and N_2O_2 as the nascent products (*rds 1*), for **1**-H(4) and **1**-H(1) the emerging products are high-energy Et_2N^- and $HN_2O_2^+$ (*rds 2*). With reference to tautomerization energies in Table 1 and the notations in Scheme 4, it is easy to see that the *minimal* free energy difference (in kcal/mol) between *rds 2* and *rds 1* is $\Delta_2G - \Delta_2G = 1.36(pK_{a1} - pK_{a2}) + \Delta_{t2}G$. Taking into account that $pK_{a1} = pK_a(R_2NH) \approx 35$ [46], $pK_{a2} = pK_a(HN_2O_2^+)$ is certainly negative, and $\Delta_{t2}G \approx 4$ kcal/mol, we estimate that the *rds 1* pathway is at least by 52 kcal/mol more favorable than any of the *rds 2* pathways. Because this number by far exceeds the activation energy of 21 kcal/mol that we have observed, there is little, if any, doubt that the amino NONOates decompose through the N5-protonated tautomer, and Eq. (5) reduces to

$$k_{mp} = k_d(5)\frac{K_{mp}}{K_a(\mathbf{1}\text{-H}(5))} \tag{6}$$

so that $k_d(5)$ and K_a(**1**-H(5)) cannot be separately obtained from the kinetic data alone. However, from Eq. (6) and the data in Table 2, we derive $k_d(5)/K_a(\mathbf{1}\text{-H}(5)) = 4 \times 10^4\ M^{-1}\ s^{-1}$. Invoking our computational data for $pK_a(\mathbf{1}\text{-H}(5)) \approx -2.8$, we estimate $k_d(5) \approx 2 \times 10^7\ s^{-1}$.

We have also investigated the $k_d(5)$ decomposition pathway computationally, and the result is shown in Fig. 6. We find that N3–N5 bond scission in **1**-H(5) requires significant activation and results in a metastable $Et_2NH\cdots N_2O_2$ complex (see Fig. S5 and Table S3 for structures and energetics of the transition states and the complex). The lowest energy decomposition pathway includes three steps: (a) equilibrium tautomerization between **1**-H(1) and **1**-H(5) occurring through intermediacy of their common conjugate base **1**, (b) N3–N5 bond scission in **1**-H(5), and (c) decomposition of the nascent $Et_2NH\cdots N_2O_2$ complex from step b. Applying the activated complex formalism to the observed k_{mp} temperature dependence, we obtain

$$k_{mp} = \frac{kT}{h}exp\left(-\frac{\Delta G^{\#}_{obs}}{RT}\right) = \frac{kT}{h}exp\left(-\frac{\Delta_{tau}G + \Delta_dG^{\#}}{RT}\right) \tag{7}$$

where $\Delta G^{\#}_{obs}$ is the experimentally observed activation free energy and the meaning of $\Delta_{tau}G$ and $\Delta_dG^{\#}$ is evident from Fig. 6. From data in Table 2, we obtain $\Delta G^{\#}_{obs} = 16.1$ kcal/mol; this number is in good agreement with the computed value for $\Delta_{tau}G + \Delta_dG^{\#} = 17.8$ kcal/mol.

Previously, Houk and co-workers [23] explored a mechanism qualitatively analogous to the one shown in Scheme 4 and derived $k_d(5) = 7.2 \times 10^{11}\ s^{-1}$ and $pK_a(\mathbf{1}\text{-H}(5)) = -6.9$ by analyzing an incomplete pH dependence of k_{obs} available only in the pH 8–5.2 range [22] (that is, without reaching the low pH "plateau"), and supported this very negative pK_a by theoretical energy computations. Thus, **1**-H(5) was described as an extremely strong acid with virtually no stability toward losing N_2O_2. In contrast, $k_d(5) \approx 2 \times 10^7\ s^{-1}$ and $pK_a(\mathbf{1}\text{-H}(5)) \approx -2.8$ obtained in the present work suggest that **1**-H(5) is a much weaker acid, whose decomposition with the N_2O_2 release is significantly activated and thus relatively slow. This large disagreement merits two brief comments. As has been mentioned above, it is impossible to obtain both $k_d(5)$ and $pK_a(\mathbf{1}\text{-H}(5))$ even from a complete k_{obs} vs pH dependence; even the $k_d(5)/K_a(\mathbf{1}\text{-H}(5))$ ratio that can be obtained from Eq. (6) is subject to a large uncertainty without the kinetic data below pH 5, such as those in Fig. 4, that include a rate plateau. Second, the values of $k_d(5)$ and $pK_a(\mathbf{1}\text{-H}(5))$ suggested by Houk and co-workers are incompatible with the key premises behind Scheme 4, which are equilibrium between tautomers and the N3–N5 bond heterolysis being the rate determining step, because it is inconceivable

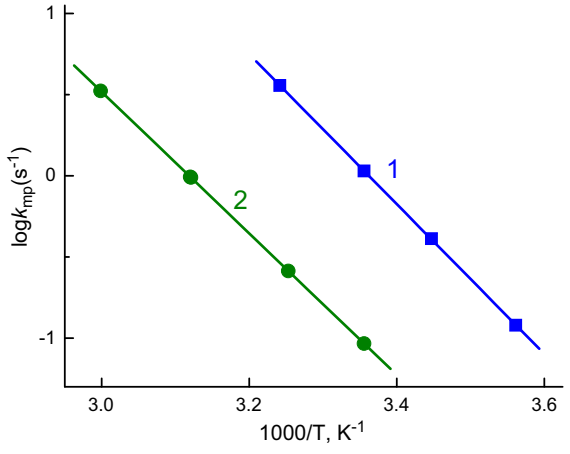

Fig. 5. Temperature dependencies in the Arrhenius coordinates of the observed decomposition rate constants for **1** (squares) and **2** (circles) at pH 2 ($HClO_4$). The activation energy (E_a) and pre-exponential factor (A) derived from the linear fits are shown in Table 2.

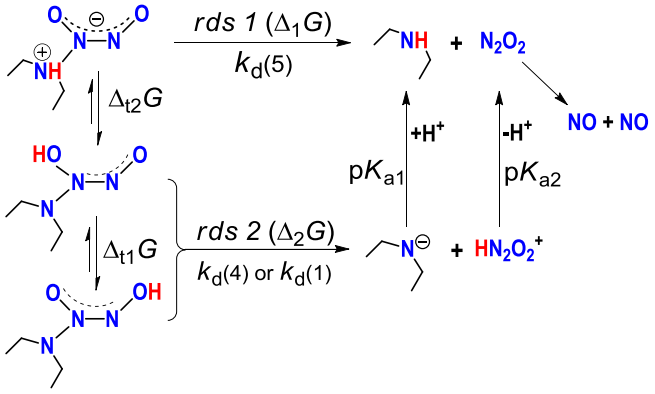

Scheme 4. Free energy relationship between tautomerization and decomposition of **1**-H.

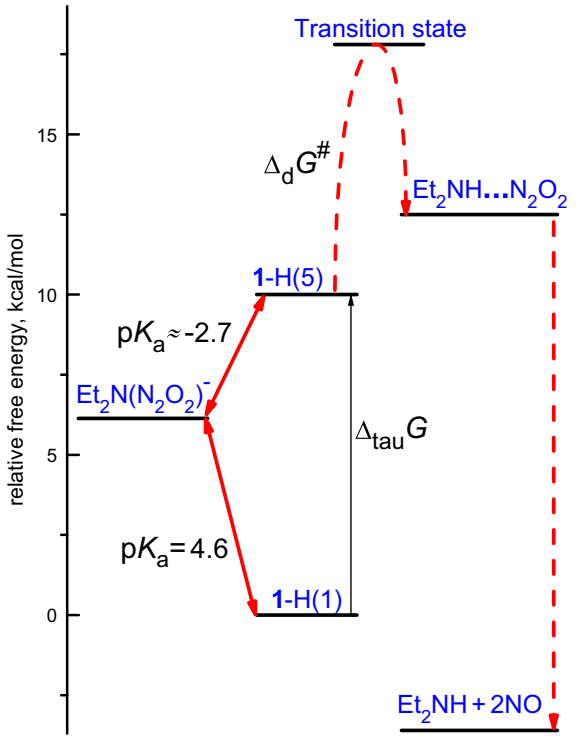

Fig. 6. Computed energy profile for the proton-initiated decomposition of **1**. Solid and dashed red arrows show the pre-equilibrium and decomposition steps, respectively. The transition state corresponds to the N3 – N5 bond scission.

that equilibration of the so strongly acidic **1**-H(5) can compete with its decomposition occurring at ~10^{12} s^{-1}. It can be shown that tautomerization **1**-H(1) → **1**-H(5) becomes rate limiting if $k_d(5)$ exceeds ~10^9 s^{-1} and pK_a(**1**-H(5)) is more negative than about −4.5 (see Scheme S1 and its discussion); thus the numerical values for $k_d(5)$ close to 10^{12} s^{-1} and pK_a(**1**-H(5)) ≈ −7 that were obtained in [23] invalidate the very mechanism that they were intended to quantitatively describe. In contrast, our values for $k_d(5)$ and pK_a(**1**-H(5)) are well within the required limits.

With the decomposition mechanism for di-protonated NONOates that becomes increasingly important at pH < 2 (Fig. 4), the situation is less clear-cut. There are 10 di-protonated tautomers and their detailed exploration in aqueous environment is computationally expensive. It is also doubtful that the second plateaus somewhere at pH < 0 in the pH-dependencies for k_{obs} in Fig. 4 can be reached and the values of k_{dp} and K_{dp} can be determined experimentally. Nevertheless, a reasonable mechanistic proposition can be made. As with the mono-protonated species, the decomposing di-protonated tautomer will probably need a proton on the N5 atom to provide for the lowest energy pathway by releasing amine, an excellent leaving group. Of the remaining sites, the O1 will probably remain the most basic after N5 has been protonated. Thus, we tend to think that the di-protonated species decompose as shown in Scheme 5. Our calculations have shown that the **1**-$H_2(1,5)^+$ tautomer does exist in water as a bound structure (Fig. S6), which makes this mechanism plausible.

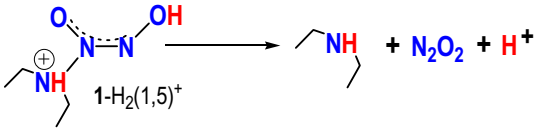

Scheme 5. Proposed structure and decomposition pathway for the **1**-$H_2(1,5)^+$ tautomer.

Overall, the experimental and computational results and their interpretation presented in this work suggest that initiation by protonation and involvement of several protonated tautomers are likely to be the common features in decomposition of NONOates. Therefore, structural and thermochemical characterization of these tautomers is a major prerequisite for molecular-level understanding of the decomposition process. Because this information is difficult, if not impossible, to obtain from experimental measurements, computational modeling becomes of significant value. Even in their uncharged, protonated state, NONOates exhibit significant intramolecular charge separation, which places a great demand on a computational model in both electronic structure and solvation treatment. We believe that our approach, based on the explicit treatment of water for the electronic structure characterization followed by the hydration energy computation through the continuum approximation, provides a reasonable practical solution to this problem. However, as with any model, theoretical predictions are not infallible and should be crosschecked with reality and the experimental data, as has been done in present work. While essential, information on the distribution of tautomers is only part of the picture because the NONOate decomposition reactions are substantially activated (Table 2). Thus, calculation of the free energy activation barriers is another place where theoretical modeling can make a substantial impact.

To illustrate these points, let us consider tautomers **1**-H(2) and **1**-H(5) from Fig. 3 and Table 1. The former can, in principle, decompose to nitrosamine and nitroxyl

$$R_2NN(O)N(H)O \rightarrow R_2NNO + HNO \quad (8)$$

but this reaction is not a major channel with R = ethyl, apparently because **1**-H(2) is higher in energy then **1**-H(5). However, it is conceivable that replacement of the ethyl by a less electron-donating group could decrease the basicity of N5 to a greater degree than that of N2, thus narrowing or even reversing the ~4 kcal/mol energy gap between **1**-H(2) and **1**-H(5); with a favorable free energy activation barrier, this change in relative basicity can lead to the predominance of HNO-producing pathway. The computational approach can certainly help with fundamental understanding of how overall reaction process can be influenced by the choice of functional groups in NONOates, and the effort in this direction is under way [47].

Acknowledgments

We thank Dr. V. Shafirovich (NYU) for valuable discussions. This research was supported by the U.S. Department of Energy, Office of Basic Energy Sciences, Division of Chemical Sciences, Geosciences, and Biosciences. Research at Brookhaven National Laboratory was carried out under contract DE-AC02-98CH10886. Research at Pacific Northwest National Laboratory was performed in part using the Molecular Science Computing Facility in the William R. Wiley Environmental Molecular Sciences Laboratory.

Appendix A. Supplementary data

Supplementary data to this article can be found online at http://dx.doi.org/10.1016/j.jinorgbio.2014.08.008. These data include MOL files and InChiKeys of the most important compounds described in this article.

References

[1] L.K. Keefer, R.W. Nims, K.M. Davies, D.A. Wink, Methods Enzymol. 268 (1996) 281–293.
[2] J.A. Hrabie, L.K. Keefer, Chem. Rev. 102 (2002) 1135–1154.
[3] J.E. Saavedra, L.K. Keefer, J. Chem. Educ. 79 (2002) 1427–1434.
[4] L.K. Keefer, Annu. Rev. Pharmacol. Toxicol. 43 (2003) 585–607.
[5] M.R. Miller, I.L. Megson, Br. J. Pharmacol. 151 (2007) 305–321.
[6] L.K. Keefer, ACS Chem. Biol. 6 (2011) 1147–1155.

[7] G.A. Poskrebyshev, V. Shafirovich, S.V. Lymar, J. Am. Chem. Soc. 126 (2004) 891–899.
[8] S.V. Lymar, V. Shafirovich, G.A. Poskrebyshev, Inorg. Chem. 44 (2005) 5212–5221.
[9] G.A. Poskrebyshev, V. Shafirovich, S.V. Lymar, J. Phys. Chem. A 112 (2008) 8295–8302.
[10] M. Valiev, S.V. Lymar, J. Phys. Chem. A 115 (2011) 12004–12010.
[11] F.T. Bonner, M.N. Hughes, Comments Inorg. Chem. 7 (1988) 215–234.
[12] V. Shafirovich, S.V. Lymar, Proc. Natl. Acad. Sci. U. S. A. 99 (2002) 7340–7345.
[13] C.M. Pavlos, H. Xu, J.P. Toscano, Free Radic. Biol. Med. 37 (2004) 745–752.
[14] S.V. Lymar, V. Shafirovich, J. Phys. Chem. B 111 (2007) 6861–6867.
[15] C.M. Maragos, D. Morley, D.A. Wink, T.M. Dunams, J.E. Saavedra, A. Hoffman, A.A. Bove, L. Isaac, J.A. Hrabie, L.K. Keefer, J. Med. Chem. 34 (1991) 3242–3247.
[16] J.A. Hrabie, J.R. Klose, D.A. Wink, L.K. Keefer, J. Org. Chem. 58 (1993) 1472–1476.
[17] A. Ramamurthi, R.S. Lewis, Chem. Res. Toxicol. 10 (1997) 408–413.
[18] K.M. Miranda, T. Katori, C.L.T. de Holding, L. Thomas, L.A. Ridnour, W.J. MeLendon, S.M. Cologna, A.S. Dutton, H.C. Champion, D. Mancardi, C.G. Tocchetti, J.E. Saavedra, L.K. Keefer, K.N. Houk, J.M. Fukuto, D.A. Kass, N. Paolocci, D.A. Wink, J. Med. Chem. 48 (2005) 8220–8228.
[19] S. Griveau, C. Dumezy, P. Goldner, F. Bedioui, Electrochem. Commun. 9 (2007) 2551–2556.
[20] Q. Li, J.R. Lancaster Jr., Nitric Oxide 21 (2009) 69–75.
[21] D.K. Taylor, I. Bytheway, D.H.R. Barton, C.A. Bayse, M.B. Hall, J. Org. Chem. 60 (1995) 435–444.
[22] K.M. Davies, D.A. Wink, J.E. Saavedra, L.K. Keefer, J. Am. Chem. Soc. 123 (2001) 5473–5481.
[23] A.S. Dutton, J.M. Fukuto, K.N. Houk, Inorg. Chem. 43 (2004) 1039–1045.
[24] A.S. Dutton, C.P. Suhrada, K.M. Miranda, D.A. Wink, J.M. Fukuto, K.N. Houk, Inorg. Chem. 45 (2006) 2448–2456.
[25] D. Andrei, D.J. Salmon, S. Donzelli, A. Wahab, J.R. Klose, M.L. Citro, J.E. Saavedra, D.A. Wink, K.M. Miranda, L.K. Keefer, J. Am. Chem. Soc. 132 (2010) 16526–16532.
[26] D.J. Salmon, C.L.T. de Holding, L. Thomas, K.V. Peterson, G.P. Goodman, J.E. Saayedra, A. Srinivasan, K.M. Davies, L.K. Keefer, K.M. Miranda, Inorg. Chem. 50 (2011) 3262–3270.
[27] M. Valiev, E.J. Bylaska, N. Govind, K. Kowalski, T.P. Straatsma, H.J.J. Van Dam, D. Wang, J. Nieplocha, E. Apra, T.L. Windus, W. de Jong, Comput. Phys. Commun. 181 (2010) 1477–1489.
[28] J. Chen, H.Y. Yin, D.Y. Wang, M. Valiev, Chem. Phys. Lett. 559 (2013) 30–34.
[29] T.T. Wang, H.Y. Yin, D.Y. Wang, M. Valiev, J. Phys. Chem. A 116 (2012) 2371–2376.
[30] H.Y. Yin, D.Y. Wang, M. Valiev, J. Phys. Chem. A 115 (2011) 12047–12052.
[31] M. Valiev, B.C. Garrett, M.K. Tsai, K. Kowalski, S.M. Kathmann, G.K. Schenter, M. Dupuis, J. Chem. Phys. 127 (2007) 051102.
[32] M. Valiev, E.J. Bylaska, M. Dupuis, P.G. Tratnyek, J. Phys. Chem. A 112 (2008) 2713–2720.
[33] A. Klamt, G. Schuurmann, J. Chem. Soc. Perkin Trans. 2 (1993) (1993) 799–805.
[34] C. Lee, W. Yang, R.G. Parr, Phys. Rev. B 37 (1988) 785–789.
[35] R. Krishnan, J.S. Binkley, R. Seeger, J.A. Pople, J. Chem. Phys. 72 (1980) 650–654.
[36] H.J.C. Berendsen, J.R. Grigera, T.P. Straatsma, J. Phys. Chem. 91 (1987) 6269–6271.
[37] G. Henkelman, B.P. Uberuaga, H. Jonsson, J. Chem. Phys. (2000) 9901–9904.
[38] R.J. Bartlett, M. Musial, Rev. Mod. Phys. 79 (2007) 291–352.
[39] E. Papajak, H.R. Leverentz, J.J. Zheng, D.G. Truhlar, J. Chem. Theory Comput. 5 (2009) 3330.
[40] E.V. Stefanovich, T.N. Truong, Chem. Phys. Lett. 244 (1995) 65–74.
[41] C.H. Arrowsmith, A. Awwal, B.A. Euser, A.J. Kresge, P.P.T. Lau, D.P. Onwood, Y.C. Tang, E.C. Young, J. Am. Chem. Soc. 113 (1991) 172–179.
[42] L.K. Keefer, J.L. Flippen-Anderson, C. George, A.P. Shanklin, T.A. Dunams, D. Christodoulou, J.E. Saavedra, E.S. Sagan, D.S. Bohle, Nitric Oxide 5 (2001) 377–394.
[43] J.E. Huheey, Inorganic Chemistry, 3rd ed. Harper & Row, New York, 1983.
[44] G.W. Stevenson, D. Williamson, J. Am. Chem. Soc. 80 (1958) 5943–5947.
[45] W.M. Haynes (Ed.), CRC Handbook of Chemistry and Physics, CRC Press, Boca Raton, FL, 2013, (Section 5, No 94).
[46] R.P. Bell, The Proton in Chemistry, Cornell University Press, Itheca, New York, 1959.
[47] Y.-N. Wang, J. Collins, R.J. Holland, L.K. Keefer, J. Ivanic, J. Phys, Chem. A 117 (2013) 6671–6677.